Hollow core-shell nanostructure supercapacitor electrodes : gap matters

Guan, Cao; Xia, Xinhui; Meng, Nan; Zeng, Zhiyuan; Cao, Xiehong; Soci, Cesare; Zhang, Hua; Fan, Hong Jin

2012

Dynamic Article Links ▶

COMMUNICATION

Hollow Core-shell Nanostructure Supercapacitor Electrodes: Gap Matters

Cao Guan[a,c], Xinhui Xia[a], Nan Meng[a], Zhiyuan Zeng[b], Xiehong Cao[b], Cesare Soci[a], Hua Zhang[b], and Hong Jin Fan*[a,c]

Hollow core-shell nanorods with a nanogap are designed and constructed with the assistance of atomic layer deposition (ALD) for energy storage applications. As a demonstration,
10 **CoO nanorods and NiO nanowalls are enclosed by a TiO$_2$ nanotube shell, forming the "wire in tube" and "wall in box" structures, respectively. A thin sacrificial layer of Al$_2$O$_3$ is deposited by ALD and removed eventually, forming a nanogap between the CoO core (or NiO nanowall) and TiO$_2$**
15 **shell. When they are tested as supercapacitor electrodes, an evident difference between the solid core-shell nanostructure and hollow ones are found; for example, the hollow structure shows ~2-4 times of capacitance compared to the solid wires. The electrochemical properties are also superior compared to**
20 **the bare nanorods without the nanotube shell. The enhancement is ascribed to the conformal hollow design which provides enlarged specific surface areas and shorter ion transport path. It is prospected that such positive nanogap effect may also exisit in other electrochemical cell**
25 **electrodes such as lithium ion batteries and fuel cells.**

Introduction

With the fossil-fuel crisis and the ever-increasing demand for high-performance portable electronic devices,
30 supercapacitor electrode materials with high specific capacitance, good rate capability and long cycling stability are needed[1-4]. However, the energy density of existing carbon-based supercapacitors is limited, generally an order of magnitude lower than that of batteries. Transitional metal
35 oxides are promising electrode materials for higher energy density as they can store more charges with pseudoreactions while carbon-based materials only store charges electrostatically at their surfaces. However, metal oxides also have problems. In a nutshell, they usually show limited
40 kninetics druing the redox reaction with ions as a result of their low electrical conductivity and low surface area compared to carbon[5-8].

In the research on metal-oxide nanostructured electrodes, several strategies are utilized to constructe high-performance
45 supercapacitors. The first is high specific surface area, that is usually manifested by a porous/hollow feature[9-20]. Large porosity provides easier electrolyte penetration and hollow center increases surface-to-bulk ratio thus more contact area between the active material and the electrolyte, leading to
50 more efficient ion transport. Furthermore, improved rate capability and cycling performance can also be achieved because these void spaces could effectively buffer the strain generated during the fast charge/discharge process.

The second way is direct growth of nanomaterials of
55 metal oxides on currect collectors[21-23]. This method ensures good mechanical adhesion and electric connection of the active material to the current collector. Also dead mass could be avoided as the polymer binders and conductive addictives are not used.

60 Another strategy is to hybridize metal oxides with carbon, conductive polymer and other metal oxides into core-shell structures. This has been proven an effective way to combine the merits of the individual components[24-27]. For example, nanostructured MnO$_2$@NiO[28], Zn$_2$SnO$_4$@MnO$_2$[24] and
65 CNT@MnO$_2$[29] have been successfully fabricated and improved electrochemical performance have been demonstrated when used as supercapacitor electrodes.

Based on above considerations, we intend to combine all these strategies into one structure by a unique rational design.
70 Herein we report a novel type of "wire in tube" electrode nanomaterial which fulfiles nearly all the above favorable requirements. ALD is employed for surface coating of a sacrificial layer of Al$_2$O$_3$ and an outer TiO$_2$ nantoube shell. ALD has been demonstrated a useful tool technique for
75 surface engineering of electrode materials[30-35]. The obtained "wire in tube" structure have the three major merits: (1) a highly porous 1D core material (CoO nanorod in this case) which is directly grown on metal foams; (2) a thin and uniform nanotube shell (TiO$_2$ in this case, but could be also
80 other materials when the respective the ALD precursors are used) providing a stabalization protection[36]; and (3) a nanogap between the core and nanotube shell could serve as "ion reservoir". As a result of this design, compared to the bare nanorod and the solid core-shell wires without gap, the "wire
85 in tube" electrode have larger surface area for electrochemical reaction, faster ion transportation and improved cyclic rentention owing to the very stable TiO$_2$ shell that protects the core. Furthermore, it is posible that the tube shell can also contribute EDLC or pseudocapacitance. Such unique core-
90 shell "wire in tube" nanoarchitecture could be generalized to

many other energy applications by hybridizing with different functionalized shell materials. Our data also verify the usefulness of ALD in nanofabrication and surface engineering of nanoscale electrode materials.

Experimental details

Material synthesis

The 3D hybrid electrode material was prepared by a three-step process, as illustrated in Figure 1. 1) The CoO precursor was synthesized on nickel foam by a hydrothermal process.For this, 2 mmol $Co(NO_3)_2 \cdot 6H_2O$, 10 mmol urea and 4 mmol NH_4F were dissolved in 50 mL deionized water, then the obtained homogeneous solution was transferred into Teflon-lined stainless steel autoclave with a piece of clean nickel foam ($20 \times 50 \times 0.1$ mm^3, with upper side protected by uniform coating of polytetrafluoroethylene tape) immersed into the reaction solution at 120 ºC for 8 h growth. 2) The nickel foam with the as-grown CoO nanostructure precursor was coated with Al_2O_3 followed by TiO_2 by ALD of different cycles using a Beneq system (TFS 200) at 120˚C. Trimethylaluminum ($Al(CH_3)_3$), $TiCl_4$ and water were used as the aluminium, titanium and oxygen source, respectively. During the deposition, the reaction chamber was maintained at 1.0 mbar with a steady N_2 steam at 200 SCCM (cubic centimeter per minute). Each ALD cycle consisted of a 300-ms precursor pulse and 1-s purging time with N_2. 3) The substrates were immersed in a 0.1 M KOH solution in order to dissolve the Al_2O_3 sandwich layer. After that, the samplew were annealed in Ar at 350 ˚C for 2 h. In the following, we use "CoOƟTiO$_2$" to denote the hollow core-shell structure, and "CoO@TiO$_2$" for the solid core-shell structure.

Similar method was used for the preparation of NiO nanowall in TiO_2 nanobox structure. The NiO nanowall precursor was prepared by chemical bath deposition with a solution of 80 ml of 1 M nickel sulfate, 60 ml of 0.25 M potassium persulfate and 20 ml of aqueous ammonia (25−28％) in a 150 ml pyrex beaker at room temperature reacted for 10 min.

Characterization

In order to show clearly the nanogap, before electron miroscopy characteriztion, the top layer of TiO_2 was etched by a reactive ion etching process[30] for 35 s in a PECVD system (Plasmatherm 790 model). A mixture gas of CF_4-O_2 (55 sccm + 5 sccm) was employed with a RF power of 175 W and chamber pressure of 55 mTorr. Samples were characterized by scanning electron microscopy (SEM, JSM-6700F, 10.0 kV) and transmission electron microscopy (TEM, JEM-2010FEF, 200 kV) equipped with an energy dispersive X-ray spectrometer (EDS). The mass of electrode materials was measured on an AX/MX/UMX Balance (METTLER TOLEDO, maximum=5.1 g; delta = 0.001 mg). Nitrogen adsorption/desorption isotherms were measured on a Micromeritics TriStar 3000 porosimeter (mesoporous characterization) and Micromeritics ASAP 2020 (microporous characterization) at 77 K. All samples were outgassed at 100 ˚C for 6 h under vacuum before measurements were recorded. The specific surface areas were calculated using the Brunauer-Emmett-Teller (BET) method.

Electrochemical measurement

Electrochemical measurements using an workstation (CHI 760D) were performed in a three-electrode electrochemical cell at room temperature using a 2 M KOH as electrolyte. The nickel foam supported nanostructure (~2 cm^2 area; CoO mass: ~3.6 mg cm^{-2}; CoOƟTiO$_2$ mass: ~4.5 mg cm^{-2}, NiO mass: ~0.5 mg cm^{-2}, and NiOƟTiO$_2$ mass: ~0.7 mg cm^{-2}) acted directly as the working electrode. A Pt plate and Hg/HgO were used as the counter electrode and the reference electrode, respectively. All potentials were referred to the reference electrode. The weight in specific capacitance (F g^{-1}) and current rate (A g^{-1}) was calculated based on the whole mass of the active materials(CoO, NiO and TiO_2), and the small contribution from the Ni foam was subtracted. The specific capacitance is calculated by $C=It/m\Delta V$ and the areal capacitance is calculated by: $C_a=I \cdot t/(\Delta V \cdot S)$, where I is the discharge current, t is the discharge time, m is the mass of the active materials, ΔV is the voltage drop upon discharging, and S is the geometrical area of the electrode. Electrochemical impedance spectroscopy (EIS) measurements were carried out by applying an AC voltage with 1 mV amplitude in a frequency range from 0.1 Hz to 100 kHz at open circuit potential.

Results and discussion

Nanostructure of wire-in-tube design

Morphologies of the core-shell hollow nanorods were examined using SEM. The bare CoO nanorods cover uniformly on the substrate surface (Figure 2a). The enlarged image (inset of Figure 2a) shows that the nanorods are highly porous. Large-scale SEM image of the sample can also be seen from supporting information (Figure S1a). The uniform growth of metal oxides by solution methods on nickel foam can be found in many literatures.[37-41] After ALD coating of an Al_2O_3/TiO_2 bilayer (ALD cycles of 80/165 were used for all the following experiments), the naowires become thicker and smoother (Figure S1b-c). After removing the Al_2O_3 layer by KOH and annealing, the structure does not collapse (Figure S1d) but its hollow nature can be hardly inspected based on SEM images. In order to disclose the hollow structure, a thin top layer was removd by ion milling. One can see clearly from Figure 2b and c the hollow core-shell structure, in which the porous CoO nanorod is enclosed by a thin tube layer with a small gap.

The hollow structure can be revealed more clearly by TEM. The porous CoO nanorod are assembled by numerous interconnected nanoparticles (Figure 2d).[42] For the CoOƟTiO$_2$, a typical TEM image in Figure 2e shows clearly that the porous CoO is enclosed by a thin and continuous layer of TiO_2 with a nanogap in between. Both the tube layer of TiO_2 and the gap layer after removal of the ALD Al_2O_3 sandwich layer are uniform in thickness, owning to the conformity of ALD.[43] Direct coating of ALD TiO_2 on the CoO nanorods resulted in solid CoO@TiO$_2$ core-shell structure without nanopgap (see TEM images in supporting material).

The atomic structure of the CoOΘTiO$_2$ nanorods were investigated by high-resolution TEM (HRTEM). From images recorded from three different areas marked in Figure 3a, the crystalline property of the sturcture can be revealed. The core CoO has a cubic lattice distance of 0.21 nm corresponding to the (200) d-spacing. The lattice fringes of the outer shell shows a distance of about 0.35 nm, which matches the (101) planes of anatase TiO$_2$. These values accord well with previous reported ones for hydrothermal grown CoO nanorods [44] and the TiO$_2$ tubes by ALD.[45] It is noted that at the relatively low deposition temperature (120°C in the case), there is no solid state reactions between the three materials towards the alloy formation.[45, 46]

The hollow core-shell structure has a higher surface areas as confirmed by BET measurement. The surface area of the bare CoO nanorods on nickel foam is 7.28 m^2 g^{-1}. After transformation to the hollow core-shell structure, it increases to 11.63 m^2 g^{-1}. In contrast, direct coating of TiO$_2$ on the porous CoO reduced the surface area to 5.63 m^2 g^{-1}. Therefore the CoOΘTiO$_2$ has a larger surface in contact with electrolyte, which would be beneficial to its electrochemical performance.

Electrochemical property of the wire-in-tube electrode

The electrochemical properties of the "wire in tube" structure was investigated in details as follows. Figure S2a show the CV curves of the three structures: CoO, CoO@TiO$_2$ and CoOΘTiO$_2$. The CoO has two pairs of redox peaks in the CV curve: $CoO + OH^- \leftrightarrow CoOOH + e^-$ and $CoOOH + OH^- \leftrightarrow CoO_2 + H_2O + e^-$, which is consistent to the previous report[47]. After direct coating of TiO$_2$, the enclosed area of the CV curve is decreased, which means less active materials reacting with the electrolyte. For the hollow core-shell CoOΘTiO$_2$, the enclosed area of its CV loop is larger than the bare CoO nanorod sample, which indicates an increased in areal capacitance. In addition, the current densities of the CoOΘTiO$_2$ hollow core-shell wires are higher than those of other counterparts, implying its better electrochemical reactivity. Although TiO$_2$ has a low pseudocapacitance[48-50], the structure of CoOΘTiO$_2$ still shows an areal capacitance 52.4 % higher than bare CoO sample, and the specific capacitance is also increased from 518.9 F g^{-1} to 633.3 F g^{-1}.

Similar results can also be obtained from charge-discharge tests (Figure 4a). At the same areal current density of 10 mA cm^{-2}, the solid core-shell CoO@TiO$_2$ has an areal specific capacitance of only 0.745 F cm^{-2}, which is only 39.8 % of that of bare CoO (1.87 F cm^{-2}). However, the hollow "wire in tube" structure has a specific capacitance of 2.85 F cm^{-2}, 3.83 times of that for the CoO@TiO$_2$. Based on the mass of the three electrodes, the specific capacitance of CoO, CoO@TiO$_2$ and CoOΘTiO$_2$ is 518.9, 187.7 and 633.3 Fg^{-1}, respectively. The charge-discharge curves of the CoO and CoOΘTiO$_2$ are shown in Figure S2b-c.

The rate capability of the CoOΘTiO$_2$ is also improved (see Figure 4b). When the current density increased form 5 to 40 mA cm^{-2}, the CoOΘTiO$_2$ has a 63.3 % capacitance retation compared to 53.9 % of CoO, which means the structure of CoOΘTiO$_2$ can better maintain the electrolyte contact for reaction even in fast charge-discharge processes.

Electrochemical Impedence Spectroscopy (EIS) is a useful method to evaluate the transport property of a electrochemical system. Results of EIS on the three materials are shown in Figure 4c. In the high frequency region, the semicircle corresponds to the charge-transfer resistance at the electrode/electrolyte interface. Structure of CoOΘTiO$_2$ shows the smallest radias, which means it is most suitable for charge transport with the electrolyte. The CoO@TiO$_2$ sample has the largest charge-transfer resistance, which is within expect since the solid TiO$_2$ shell retards the charge transfer. In the low frequency regime, CoOΘTiO$_2$ also displays a more ideal straight line along the imaginary axis, which demonstrates its low diffusion resistance. The low diffusion and electron-transfer resistances of the CoOΘTiO$_2$ revealed by EIS measurement is in good accordance with its electrochemical performance above.

Finally, as one of key issues for supercapacitor electrode materials, the cycling stability has been tested for the two electrodes (Figure 4d). The CoO itself has a very good stablity (89.7 % capacitance retation after 5000 cycles at 10 mA cm^{-2}), yet the CoOΘTiO$_2$ shows a slightly better capcitance retention (95.1 % after 5000 cycles) at a higher current density (20 mA cm^{-2}).

We now discuss the mechanisms of the enhancement in psuedocapacitive performance of the "wire in tube" structure. Three possible factors might play the role. First, the nanogap effectively creates a spatial confinement to the electrolyte between the CoO core and ALD shell. Within this gap, a close contact between CoO and electrolyte is ensured enabling a rapid ion transport. The gap serves as an ''ion reservoir'' preserving a relatively stable supply of OH$^-$ even at high current densities. This may explain the improved rate capability of CoOΘTiO$_2$, which is also supported by the fact that the capacitance increase is more evident at higher current densities: (71.7 % improvement with respect to the CoO at a high current density of 40 mA cm^{-2}, see Fig. 4b).

As for the solid core-shell wires, the dense ALD TiO$_2$ layer creates a diffusion barrier (but not block) for the OH$^-$ ions to reach the CoO core, as demonstrated by EIS result. This explains why the CoO@TiO$_2$ sample has the largest charge-transfer resistance.

Second, the specific surface area is increased due to the thin nanotbue wall. In general, a conformal coating of shell material can increase the surface area several times[51]. If the TiO$_2$ nanotube shell is connected to the CoO core at any point, it effectively contributes to pseudocapacitance in a similar way to the AC-based EDLCs[50], and the physical charge on the wall of TiO$_2$ shell can transport eventually to the current collector.

Third, TiO$_2$ is a quite stable electrochemical system (Note the recent increasing interests in nano TiO$_2$ in Li-ion battry[52, 53]). The thin and conformal ALD TiO$_2$ shell protects the core materials from structrual deterioration during prolonged charge/discharge cycles. This may explain the improved capacity rentention of the hollow core-shell CoOΘTiO$_2$ nanorods comapred to the bare CoO nanorods (Figure 4d).

By changing the ALD cycles of Al$_2$O$_3$ and TiO$_2$, several

"wire in tube" structures with different thickness of hollow layer and tube layer can be obtained (typical TEM images can be seen from Figure S3a-f). All the "wire in tube" structures shows improved performance in charge-discharge tests than the CoO nanorods alone, and the structure with 20/110 ALD cycles of Al_2O_3/TiO_2 gives the largest areal capacitance (see Figure S3g).

Wall-in-box nanostructured electrode

To check the generality of the nanogap design, another hollow core-shell structure of "wall in box" was fabricated and tested. Figure 5a shows the SEM image of the vertical aligned, interconnected NiO nanowalls. After the similar treatment procedure to the above CoO nanorods (i.e., ALD coatings of Al_2O_3 and TiO_2 followed by removal of Al_2O_3), the NiO nanowalls become thicker (see Figure 5b). After ion milling, the nanogap can be clearly seen (inset of Figure 5b). The NiO nanowall in TiO_2 nanobox (denoted by $NiO\Theta TiO_2$) also showed an increased areal capacitancey, as illurstrated by CV and CD results (in Figure 5c-d). In addition, the rate capability of $NiO\Theta TiO_2$ has also increased as it shows a 64.3% capacitance retention when the current increased 10 times, compared to 58.4% of the bare NiO nanowall (see Figure S4a). The enhanced cycling stability is also achieved as shown in Figure S4b. All these improvements are in consistent with that of the porous nanorods, and further corroborate the advantage of the hollow core-shell structure design.

It is noteworthy that in this hollow electrode design, the materials for the gap layer and outer shell are not limited to Al_2O_3 and TiO_2, respecitvely. In particular, the TiO_2 shell could be replaced with carbon, or more electrochemical active oxides such as NiO and Co_3O_4. Better performance is expected if such psuedocapacitive shell can be also coated by ALD.

In conclusion, we have proposed and demonstrated a general concept of the "gapped core-shell nanostructures" for electrochemical energy storage application. With assistance by ALD, "wire in tube" and "wall in box" structures of CoO/TiO_2 are fabricated and tested. The hollow core-shell electrode with nanogap show evidently higher areal capacitance than the solid core-shell nanorods without gap, as well as improved rate capability and cycling ability. It is proposed that the nanogap provides increased reaction area and facilitates the electrolyte contact with the active material. In addition, the outlayer tube layer also perserves the structure integrity after long-time cycling. Such hollow core-shell nanostructure represents an effective way to improve the electrochemical of metal oxide-based supercapacitors. Further improvement in areal capacitance can be expected by choosing more electrochemical active shell material (such as NiO) and fine adjustment of the gap thickness.

Acknowledgement

Notes and references

a Division of Physics and Applied Physics, School of Physical and Mathematical Sciences, Nanyang Technological University, 21 Nanyang Link, 637371 Singapore. Email: fanhj@ntu.edu.sg
b School of Materials Science and Engineering, Nanyang Technological University, 639798 Singapore.
c Energy Research Institute @ NTU (ERIAN), 50 Nanyang Drive, 637553 Singapore.

1. C. Liu, F. Li, L.-P. Ma and H.-M. Cheng, *Adv. Mater.*, 2010, **22**, E28-E62.
2. G. Wang, L. Zhang and J. Zhang, *Chem. Soc. Rev.*, 2012, **41**.
3. P. Simon and Y. Gogotsi, *Nat Mater*, 2008, **7**, 845-854.
4. P. J. Hall, M. Mirzaeian, S. I. Fletcher, F. B. Sillars, A. J. R. Rennie, G. O. Shitta-Bey, G. Wilson, A. Cruden and R. Carter, *Energy Environ. Sci.*, 2010, **3**, 1238-1251.
5. X. Zhao, B. M. Sanchez, P. J. Dobson and P. S. Grant, *Nanoscale*, 2011, **3**, 839-855.
6. Z.-S. Wu, G. Zhou, L.-C. Yin, W. Ren, F. Li and H.-M. Cheng, *Nano Energy*, 2012, **1**, 107-131.
7. W. Deng, X. Ji, Q. Chen and C. E. Banks, *RSC Adv.*, 2011, **1**, 1171-1178.
8. G. Lota, K. Fic and E. Frackowiak, *Energy Environ. Sci.*, 2011, **4**, 1592-1605.
9. X. Lai, J. E. Halpert and D. Wang, *Energy Environ. Sci.*, 2012, **5**, 5604-5618.
10. C.-Y. Cao, W. Guo, Z.-M. Cui, W.-G. Song and W. Cai, *J. Mater. Chem.*, 2011, **21**, 3204-3209.
11. S. Ding, T. Zhu, J. S. Chen, Z. Wang, C. Yuan and X. W. Lou, *J. Mater. Chem.*, 2011, **21**, 6602-6606.
12. Z. Lu, Z. Chang, W. Zhu and X. Sun, *Chem. Commun.*, 2011, **47**, 9651-9653.
13. M. Xu, L. Kong, W. Zhou and H. Li, *J. Phys. Chem. C*, 2007, **111**, 19141-19147.
14. X. Zhang, W. Shi, J. Zhu, W. Zhao, J. Ma, S. Mhaisalkar, T. Maria, Y. Yang, H. Zhang, H. Hng and Q. Yan, *Nano Research*, 2010, **3**, 643-652.
15. X.-H. Xia, J.-P. Tu, Y.-J. Mai, X.-L. Wang, C.-D. Gu and X.-B. Zhao, *J. Mater. Chem.*, 2011, **21**, 9319-9325.
16. C. Guan, X. Li, Z. Wang, X. Cao, C. Soci, H. Zhang and H. J. Fan, *Adv. Mater.*, 2012, n/a-n/a.
17. J. Zhu, W. Shi, N. Xiao, X. Rui, H. Tan, X. Lu, H. H. Hng, J. Ma and Q. Yan, *ACS Appl. Mater. Interfaces*, 2012, **4**, 2769-2774.
18. Z. Li, X. Lai, H. Wang, D. Mao, C. Xing and D. Wang, *J. Phys. Chem. C*, 2009, **113**, 2792-2797.
19. W. Xia, W. Meng, R. Yu, X. Xing, D. Wang, Y. Chen and M. Takano, *Chem. Lett.*, 2006, **35**, 656-657.
20. H. Guan, X. Wang, H. Li, C. Zhi, T. Zhai, Y. Bando and D. Golberg, *Chem. Commun.*, 2012, **48**, 4878-4880.
21. J. Jiang, J. P. Liu, X. T. Huang, Y. Y. Li, R. M. Ding, X. X. Ji, Y. Y. Hu, Q. B. Chi and Z. H. Zhu, *Crystal Growth & Design*, 2009, **10**, 70-75.
22. J. Zhu, J. Jiang, J. Liu, R. Ding, H. Ding, Y. Feng, G. Wei and X. Huang, *J. Solid State Chem.*, 2011, **184**, 578-583.

23.   L. Yang, S. Cheng, Y. Ding, X. Zhu, Z. L. Wang and M. Liu, *Nano Lett.*, 2011, **12**, 321-325.

24.   G. Yu, L. Hu, M. Vosgueritchian, H. Wang, X. Xie, J. R. McDonough, X. Cui, Y. Cui and Z. Bao, *Nano Lett.*, 2011, **11**, 2905-2911.

25.   L. Bao, J. Zang and X. Li, *Nano Lett.*, 2011, **11**, 1215-1220.

26.   H. Wang, H. S. Casalongue, Y. Liang and H. Dai, *J. Am. Chem. Soc.*, 2010, **132**, 7472-7477.

27.   X. Cao, Y. Shi, W. Shi, G. Lu, X. Huang, Q. Yan, Q. Zhang and H. Zhang, *Small*, 2011, **7**, 3163-3168.

28.   J. Liu, J. Jiang, M. Bosman and H. J. Fan, *J. Mater. Chem.*, 2012, **22**, 2419-2426.

29.   S. W. Lee, J. Kim, S. Chen, P. T. Hammond and Y. Shao-Horn, *ACS Nano*, 2010, **4**, 3889-3896.

30.   L. K. Tan, M. A. S. Chong and H. Gao, *J. Phys. Chem. C*, 2007, **112**, 69-73.

31.   I. D. Scott, Y. S. Jung, A. S. Cavanagh, Y. Yan, A. C. Dillon, S. M. George and S.-H. Lee, *Nano Lett.*, 2010, **11**, 414-418.

32.   S. Boukhalfa, K. Evanoff and G. Yushin, *Energy Environ. Sci.*, 2012.

33.   X. Li, X. Meng, J. Liu, D. Geng, Y. Zhang, M. N. Banis, Y. Li, J. Yang, R. Li, X. Sun, M. Cai and M. W. Verbrugge, *Adv. Funct. Mater.*, 2012, **22**, 1647-1654.

34.   Y. S. Jung, A. S. Cavanagh, L. A. Riley, S.-H. Kang, A. C. Dillon, M. D. Groner, S. M. George and S.-H. Lee, *Adv. Mater.*, 2010, **22**, 2172-2176.

35.   J. W. Elam, D. Routkevitch, P. P. Mardilovich and S. M. George, *Chem. Mater.*, 2003, **15**, 3507-3517.

36.   G. Yu, L. Hu, N. Liu, H. Wang, M. Vosgueritchian, Y. Yang, Y. Cui and Z. Bao, *Nano Lett.*, 2011, **11**, 4438-4442.

37.   X.-H. Xia, J.-P. Tu, Y.-Q. Zhang, Y.-J. Mai, X.-L. Wang, C.-D. Gu and X.-B. Zhao, *RSC Adv.*, 2012, **2**, 1835-1841.

38.   X.-H. Xia, J.-P. Tu, X.-L. Wang, C.-D. Gu and X.-B. Zhao, *Chem. Commun.*, 2011, **47**, 5786-5788.

39.   X. Qing, S. Liu, K. Huang, K. Lv, Y. Yang, Z. Lu, D. Fang and X. Liang, *Electrochim. Acta*, 2011, **56**, 4985-4991.

40.   Y. Gao, S. Chen, D. Cao, G. Wang and J. Yin, *J. Power Sources*, 2010, **195**, 1757-1760.

41.   Q. Yang, Z. Lu, Z. Chang, W. Zhu, J. Sun, J. Liu, X. Sun and X. Duan, *RSC Adv.*, 2012, **2**.

42.   J. Liu, J. Jiang, C. Cheng, H. Li, J. Zhang, H. Gong and H. J. Fan, *Adv. Mater.*, 2011, **23**, 2076-2081.

43.   T. R. B. Foong, Y. Shen, X. Hu and A. Sellinger, *Adv. Funct. Mater.*, 2010, **20**, 1390-1396.

44.   J. Jiang, J. Liu, R. Ding, X. Ji, Y. Hu, X. Li, A. Hu, F. Wu, Z. Zhu and X. Huang, *J. Phys. Chem. C*, 2009, **114**, 929-932.

45.   C. Bae, Y. Yoon, H. Yoo, D. Han, J. Cho, B. H. Lee, M. M. Sung, M. Lee, J. Kim and H. Shin, *Chem. Mater.*, 2009, **21**, 2574-2576.

46.   X. Chu, X. Liu, G. Wang and G. Meng, *Mater. Res. Bull.*, 1999, **34**, 1789-1795.

47.   C. Guan, J. Liu, C. Cheng, H. Li, X. Li, W. Zhou, H. Zhang and H. J. Fan, *Energy Environ. Sci.*, 2011, **4**, 4496-4499.

48.   X. Lu, G. Wang, T. Zhai, M. Yu, J. Gan, Y. Tong and Y. Li, *Nano Lett.*, 2012.

49.   J. Wang, J. Polleux, J. Lim and B. Dunn, *J. Phys. Chem. C*, 2007, **111**, 14925-14931.

50.   M. S. Kim, T.-W. Lee and J. H. Park, *J. Electrochem. Soc.*, 2009, **156**, A584-A588.

51.   D. Gu, H. Baumgart, T. M. Abdel-Fattah and G. Namkoong, *ACS Nano*, 2010, **4**, 753-758.

52.   Z. Hong, M. Wei, T. Lan, L. Jiang and G. Cao, *Energy Environ. Sci.*, 2012.

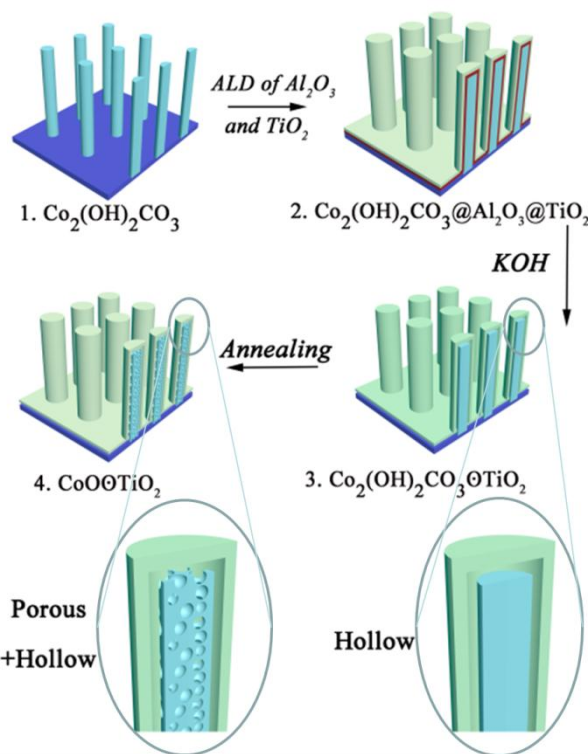53.   Z. Chen, D. Zhang, X. Wang, X. Jia, F. Wei, H. Li and Y. Lu, *Adv. Mater.*, 2012, n/a-n/a.

Figure 1. Illustration of the fabrication process of the "wire in tube" strucrure of CoO⊖TiO₂.
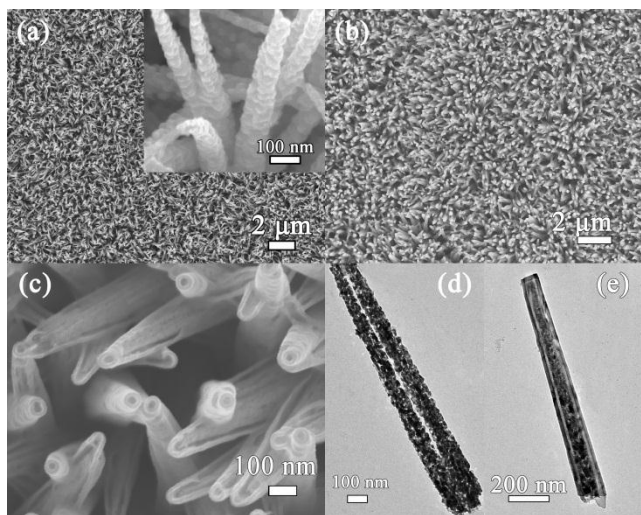
Figure 2. SEM images of (a) CoO nanorod, (b-c) "wire in tube" structure of CoOϴTiO$_2$. TEM images of (d) two CoO nanorods, and (e) "wire in tube" structure of CoOϴTiO$_2$.
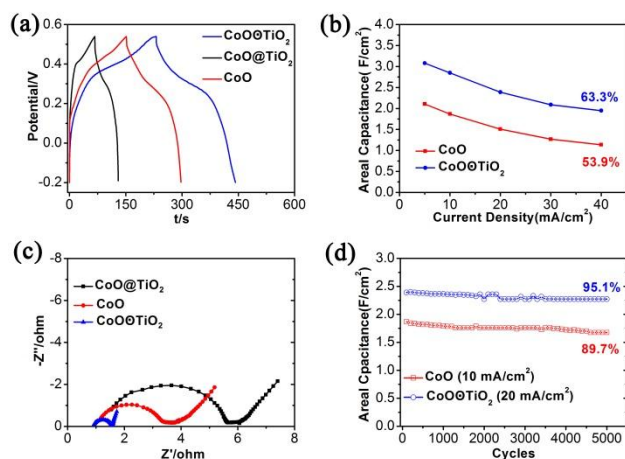
5

Figure 4. (a) Charge-discharge curve of the three structures (CoO, CoO@TiO$_2$ and CoOϴTiO$_2$) at the same current density of 10 mA cm^{-2}. (b) Rate capability of the CoO and CoOϴTiO$_2$. The
25 percentage numbers denote the capacitance retention when the current is increased from 5 to 40 mA cm^{-2}. (c) Electrochemical impedence spectroscopy of the three structures. (d) Cycling stability of the CoO and CoOϴTiO$_2$. The percentage numbers denote the capacitance retention after 5000 cycles of charge-
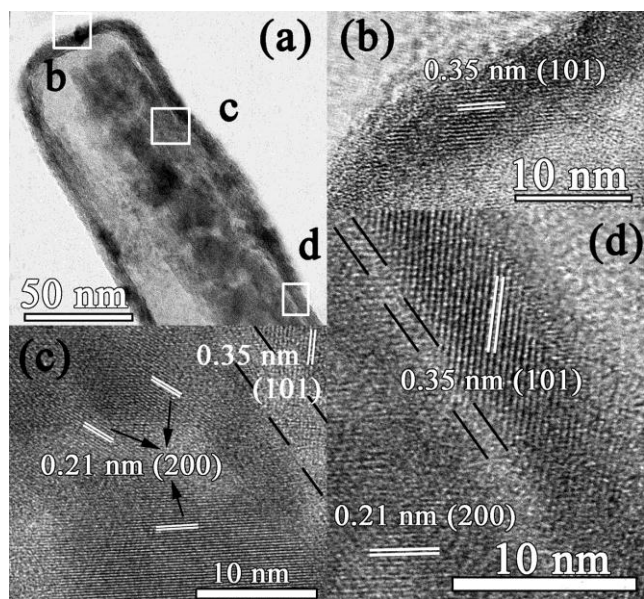30 discharge.

10

Figure 3. HRTEM characterizaton of a typical CoOϴTiO$_2$ "wire in tube" structure.
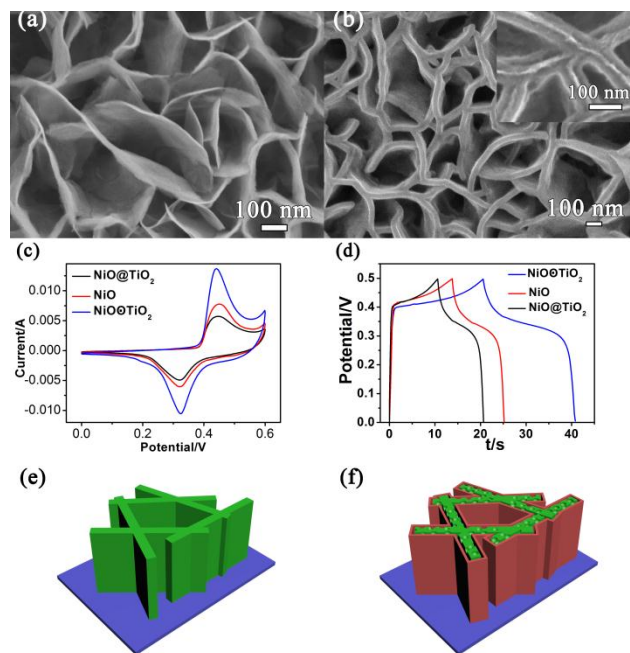
15

Figure 5. SEM images of (a) NiO nanowall, and (b) "wall in box"
35 structure of NiOϴTiO$_2$. (c) CV and (d) Charge-discharge curve of the three structures (NiO, NiO@TiO$_2$ and NiϴTiO$_2$). (e-f) Schematics of the NiO nanowall and NiOϴTiO$_2$ wall-in-wall structure.

40

20